NANO LETTERS

2005
Vol. 5, No. 10
2029−2033

Disorder Effects in Focused-Ion-Beam-Deposited Pt Contacts on GaN Nanowires

C. Y. Nam, D. Tham, and J. E. Fischer*

Department of Materials Science and Engineering, University of Pennsylvania, 3231 Walnut Street, Philadelphia, Pennsylvania 19104-6272

Received August 9, 2005; Revised Manuscript Received September 12, 2005

ABSTRACT

The current–bias (*I–V*) characteristics at various temperatures, *T*, of focused-ion-beam (FIB)-deposited Pt contacts on GaN nanowires evolves from low-resistance ohmic (linear *I–V*) to rectifying as the diameter increases, and both exhibit strongly nonmetallic *T*-dependence. The small-diameter (66 nm) *T*-dependent resistance is explained by two-dimensional variable range hopping with a small characteristic energy, ensuring low resistance at 300 K. For large diameters (184 nm), back-to-back Schottky barriers explain the nonlinear *I–V* at all *T* values and permit an estimate of doping concentration from the bias-dependent barrier height. Both behaviors can be understood by accounting for the role of FIB-induced amorphization of GaN underneath the contact, as confirmed by cross-sectional transmission electron microscopy.

Extensive research on one-dimensional (1D) nanowires (NWs) has been undertaken in the past few years. The main interest stems from enhanced physical properties at reduced dimensionality and size, such as quantum confinement.[1] GaN is an important direct and wide band gap semiconductor (3.4 eV in bulk wurtzite) for its applications in blue lasers and light-emitting diodes[2] and high-power transistors.[3] Quantum confinement is of particular interest in GaN NW because the optical efficiency and lasing threshold should be enhanced if the system is smaller than the excition radius.[4] Accordingly, many researchers reported the synthesis and device applications of GaN NWs.[5−9] In this letter, unique diameter-dependent contact conduction mechanisms are studied on focused-ion-beam (FIB)-Pt contacted GaN NW. GaN NW is grown by the thermal reaction of Ga_2O_3 and NH_3 using an Au/Pd catalyst in a quartz tube furnace and dry-transferring it onto SiO_x/Si (or SiN_x/Si) chips.[10,11] FIB-Pt contacts are deposited directly onto the NW by decomposing a trimethylcyclopentadienyl-platinum ($((CH_3)_3CH_3C_5H_4Pt)$) vapor precursor using a 30 kV Ga^+ ion beam with a total dose of $\sim 4 \times 10^{16}$ cm^{-2}.[10] At low *T*, conduction through all diameter wires is limited by the contacts. We investigate two conduction regimes and their origins on different diameter NWs, from *T*-dependent current−voltage (*I*−*V*) characteristics coupled with high-resolution transmission electron microscopy (TEM, JEOL 2010F) in a FIB-sectioned cross-sectional FIB-Pt contact specimen.

The work function of Pt ($\Phi_{m,Pt}$) and the electron affinity of GaN (χ_{GaN}) are 5.65 and 4.1 eV, respectively.[12] In the absence of interface states, the ideal barrier height (Φ_{Bo}) on n-type GaN is thus 1.55 eV. Pt is known to form a Schottky barrier on "bulk" n-GaN.[12] No intentional doping is performed in our experiment, so the NWs are presumed n-type because of the often observed autodoping by O or Si.[13,14] We verified that sputtered Pt contacts are consistently rectifying and highly resistive on our NW.[10] In contrast and much to our surprise, the FIB-Pt contacts have decades smaller resistance, with linear *I*−*V* characteristics observed from the smallest-diameter NW. Figure 1a shows 184-nm-diameter *I*−*V* curves from 40 to 300 K. The contacts are rectifying in both directions at all *T*, whereas the effective, or zero-bias, resistivity ρ (two-probe) is only 6.4 Ωcm at 300 K. The *I*−*V*−*T* behavior is totally different for smaller diameters. Figure 1b is the *I*−*V*−*T* plot of the 66-nm-diameter NW. The *I*−*V* is now linear in the whole *T* range, and ρ is even smaller, 0.06 Ωcm at 300 K. The nonlinear or linear *I*−*V* for the large- or small-diameter NW, respectively, was observed consistently in many samples.

We first discuss the nonlinear *I*−*V*−*T* characteristics of the large-diameter NW. In light of the typical Schottky barrier formation by Pt on n-type GaN, our two-terminal device most likely consists of back-to-back Schottky junctions. When biased, the total current is limited by the junction on the higher potential side for either polarity. Electrons "see" the barrier from the metal side; the barrier height is nominally constant and little current flows until breakdown. Assuming thermionic emission, the appropriate *I*−*V*−*T* relation is that of a reverse-biased Schottky diode. The barrier height decreases and current increases with increasing bias because

* Corresponding author. E-mail: fischer@seas.upenn.edu.

10.1021/nl0515697 CCC: $30.25
Published on Web 09/24/2005

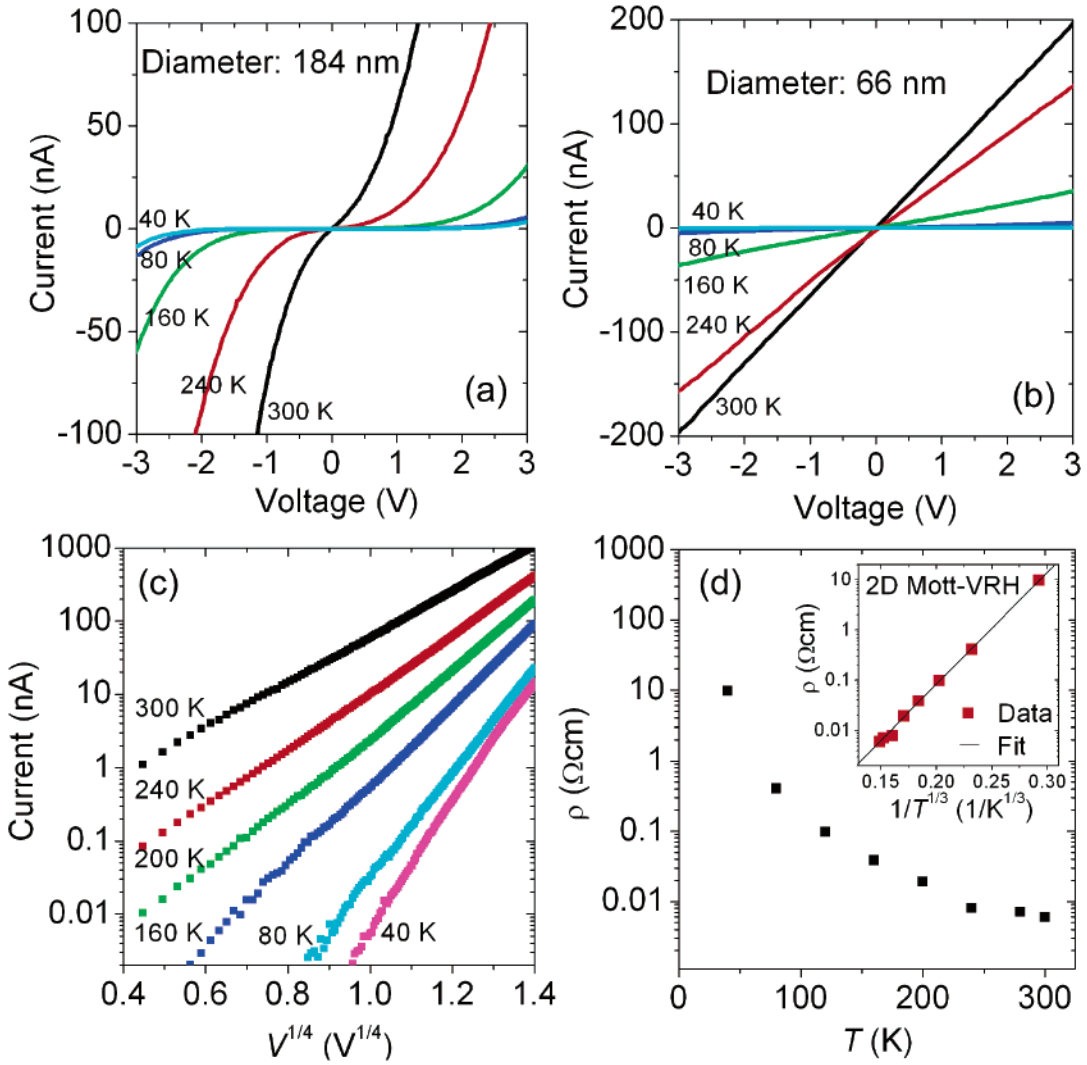

Figure 1. Two-probe $I-V$ characteristics measured from 40 to 300 K on FIB-Pt contacted GaN NW (a−c) and a model fit (d). (a) For a 184-nm-diameter NW, $I-V$ is nonlinear and the zero bias resistance increases rapidly with decreasing T. (b) For a 66-nm-diameter NW, $I-V$ is linear, the zero bias resistance also increases rapidly with decreasing T, and the apparent zero-bias resistivity ρ at 300 K is two decades smaller (0.06 Ωcm) than that for the 184-nm NW (6.4 Ωcm). Intermediate diameters give intermediate values of ρ. Plotted in c is log(I) vs $V^{1/4}$ for the 184-nm-diameter NW; the linear behavior at and above 160 K is consistent with back-to-back Schottky barrier contacts. Conversely, the T-dependent behavior of the 66-nm-diameter NW shown in d suggests 2D variable range hopping. See the text for details.

of the image force according to the following[15]

$$I = AA^{**}T^2 \exp\left(\frac{-q\Phi_{BE}}{k_B T}\right) \quad (1)$$

where

$$\Phi_{BE} = \Phi_{Bo} - \sqrt{\frac{qE}{4\pi\epsilon_S}} \quad (2)$$

and

$$E = \sqrt{\frac{2qN_D}{\epsilon_S}\left(V + \Phi_{bi} - \frac{k_B T}{q}\right)} \quad (3)$$

where A is the contact area, A^{**} is the effective Richardson constant, Φ_{BE} is the effective barrier height, Φ_{Bo} is the ideal barrier height in the absence of image force, E is the maximum electric field at the junction, ϵ_s and N_D are the dielectric constant and doping concentration of GaN, and Φ_{bi} is the built-in potential. Several useful relations can be derived from eqs 1−3. First, ln(I) is linear in $V^{1/4}$ at all T values for which the Schottky model is valid. Second, Φ_{BE} can be obtained as a function of V from the slope of an activation-energy plot of ln(I/T^2) versus $1/T$. This holds for relatively high T values where A^{**} and Φ_{BE} are T-independent.[15]

The 184-nm-diameter device behavior is well described by the back-to-back Schottky barrier model. Figure 1c shows that log(I) versus $V^{1/4}$ is linear over the whole bias range for $T > 160$ K, with small but significant deviations at lower temperatures because of thermal variations of A^{**} and Φ_{BE}. The bias-dependent Φ_{BE} is calculated from the slope of log(I/T^2) versus $1/T$ as shown in Figure 2a. Figure 2b shows

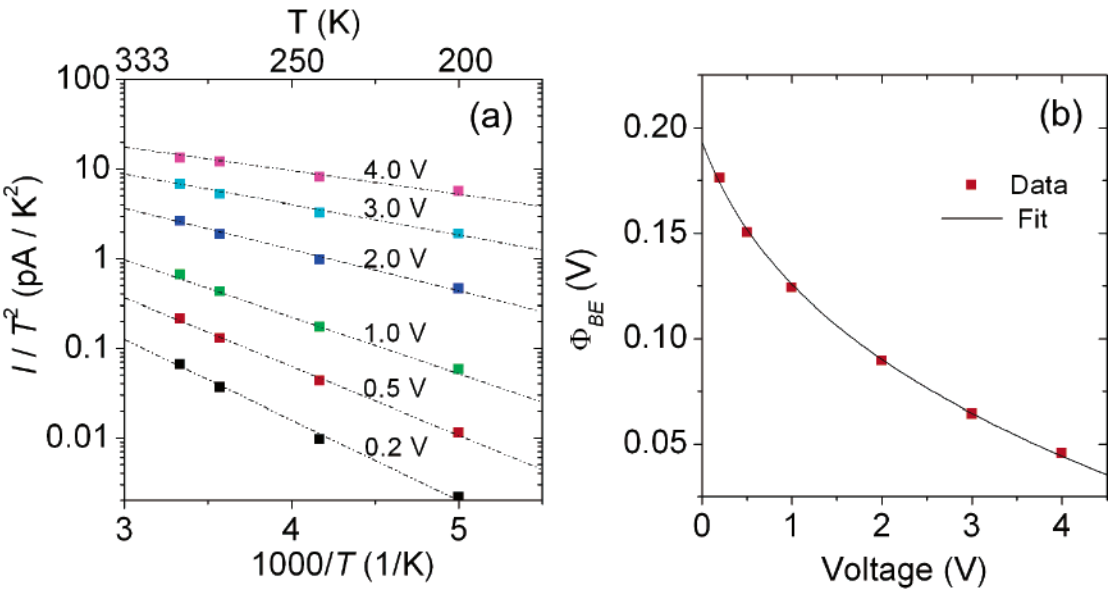

Figure 2. (a) $\log(I/T^2)$ vs $1/T$ plots at several bias values for the 184-nm-diameter NW. The slope remains negative for the whole bias range, consistent with positive barrier height. (b) Bias dependence of the effective barrier height, Φ_{BE}, in the range of $0.2 < V < 4$ V, derived from the slopes in a. Φ_{BE} decreases with increasing bias (filled symbols). A fit to eq 4 (solid curve) shows that the bias dependence arises from image force-induced barrier height lowering.

that Φ_{BE} decreases from 0.18 to 0.04 eV with increasing bias and is much smaller than the ideal value, 1.55 eV. The solid curve gives a good account of the bias-dependent barrier height reduction and will be described later.

The linear $I-V-T$ characteristics of the 66-nm-diameter NW can be explained by variable range hopping (VRH). As shown in Figure 1b, $I-V$ is linear in the whole T range, indicating zero barrier height. The main part of Figure 1d shows the measured two-probe ρ versus T. We find diverging ρ as T goes to zero with ~3 decades increase from 300 to 40 K, suggestive of VRH conduction in a disordered semiconductor. According to Mott,[16] the VRH resistivity $\rho \propto \exp[(T^*/T)^P]$ where p is 1/4, 1/3, or 1/2 for hopping in 3-, 2-, and 1D, respectively. The energy scale of the localization is defined by $k_BT^* = 2^{1/p}\Delta_{NN}/2p(1-p)$ where Δ_{NN} is a characteristic energy separation between nearest-neighbor states.[17] The inset of Figure 1d shows the data and fit to $\log(\rho)$ versus $1/T^{1/3}$ (2D VRH). The fit is excellent in the whole range, and the estimated Δ_{NN} is ~0.4 eV. Other dimensionalities gave unphysically large Δ_{NN}, and no dimensionality gave a reasonable VRH fit to the 184-nm-diameter data.

The above analysis assumes that the measured two-probe ρ is dominated by the contacts, with the intervening segment of NW offering no significant resistance to the current flow. We show next that the ρ versus T behavior is indeed representative of the contacts because the NW is heavily doped and its contribution to ρ is small and independent of T.[18]

Measuring the dopant concentration, N_D, in NWs is in general nontrivial. Transverse electrodes for Hall effect measurement are complicated by the wire geometry, and our GaN NW devices exhibit no gate response from which N_D could be estimated.[7] In the current work, the bias-dependent barrier height lowering (Φ_{BE} vs V) of the large-diameter NW allows us to estimate N_D. Solving eqs 2 and 3 for Φ_{BE} yields

$$\Phi_{BE} = \Phi_{Bo} - \sqrt{\frac{q}{4\pi\epsilon_S}}\sqrt{\frac{2qN_D}{\epsilon_S}\left(V + \Phi_{bi} - \frac{k_BT}{q}\right)} \quad (4)$$

The thermal energy, k_BT, is small compared to V and Φ_{bi} and can be neglected for all T. Substituting $\Phi_{bi} = \Phi_{Bo} - k_BT\ln(N_C/N_D) \approx \Phi_{Bo}$, where N_C is the effective conduction band density of states, Φ_{BE} simplifies to

$$\Phi_{BE} \cong \Phi_{Bo} - \sqrt{\frac{q}{4\pi\epsilon_S}}\sqrt{\frac{2qN_D}{\epsilon_S}(V + \Phi_{Bo})} \quad (5)$$

The Φ_{BE} versus V data and its least-squares fit to eq 5 with Φ_{Bo} and N_D as free parameters are shown in Figure 2b. The fit is excellent with $\Phi_{Bo} = 0.37$ eV and $N_D = 2.3 \times 10^{19}$ cm^{-3}. Recall that Φ_{Bo} is the ideal barrier height in the absence of image force, and is different from Φ_{BE} at zero bias (~0.19 eV). The large value of N_D explains why we observe no gate response in the gate voltage in the V_G range ±20 V. In a NW field-effect transistor (FET), the turn-off gate voltage, $V_{G,off}$, is proportional to N_D:[7] $V_{G,off} = N_D\, qr^2\, \ln(2h/r)/2\epsilon_{di}$, where r, h, and ϵ_{di} are the NW radius, thickness, and dielectric constant of the oxide. For a 100-nm GaN NW on 100-nm SiO_x, $V_{G,off}$ is ~700 V, 30 times greater than our experimental limit.

Finally, we consider the structural origin of the different contact transport mechanisms and their dependence on diameter, in terms of the unique role of FIB-induced disorder. Recall that Φ_{BE} in the large-diameter NW is much lower (0.04−0.18 eV) than the ideal Schottky barrier height (1.55 eV) or the measured barrier height of thin-film Pt on bulk n-GaN (1.13−1.27 eV).[12] In compound semiconductors,

Fermi level (E_F) pinning tends to be significant because of surface or interface states,[15] so the actual barrier height is independent of Φ_m. Irradiation by focused Ga^+ beams is known to create N-vacancies[19] and/or amorphization[20] in GaN NW. Similar disorder is expected underneath the Pt contacts in the 30-kV Ga^+ beam Pt deposition process because the direct ion beam irradiation of NW is still present. It is known that two groups of N-vacancy-related states, created by high-energy electron beam irradiation[21] or by plasma etching,[22] typically lie 25−70 meV or 0.5 eV below the conduction band edge (E_C) in bulk GaN. We thus propose that the low barrier height arises from E_F pinning at these N-vacancy-related interface states. Pinning is also possible at shallow amorphization-induced localized states near E_C.[16] Unlike amorphous (a-) Si or Ge, a-GaN has no deep midgap states.[23,24]

Cross-sectional TEM analysis directly confirms the existence of FIB-induced disorder under the contacts. Details will be published elsewhere.[25] Figure 3a shows a bright-field scanning TEM (STEM) image of an FIB-Pt contact cross-section. High-resolution imaging (Figure 3b and c) unambiguously reveals a 2−3-nm-thick band of amorphized GaN directly underneath the contact. The crystallinity in the core of the NW is also significantly disrupted, as indicated by the diffuse diffraction spots. The top ~30 nm of GaN has been sputtered off (not shown). These observations are consistent with the proposal that E_F pinning and low barrier height are due to localized states in the amorphized GaN.

The onset of VRH conduction and ohmic behavior with decreasing NW diameter, d, is understood in terms of the increasing fraction of disordered GaN under the contact. The characteristic depth of ion-beam-induced disorder is observed to be 20−40 nm.[25] This means that the large-diameter wires, which do not exhibit VRH conduction, retain largely intact crystalline cores in which the transport is not strongly affected by disorder. This provides a natural explanation for the different $I-V-T$ behaviors for thick and thin wires; in the thinner ones, VRH is the consequence of disorder dominating transport through the beam-damaged contacts.

The analogy to the increase of surface-to-volume ratio with decreasing d gives an explicit explanation. The contact area normal to the current flow covers the disordered layer completely. The volume fraction of the disordered region is proportional to $1/d$ because the surface-to-volume ratio is $\sim 1/d$ and the disordered layer thickness is the same for all wires because of identical FIB conditions: as d decreases, the fraction increases, and $d = 66$ nm is then small enough that the entire electron flow occurs by VRH. The aforementioned sputtering during deposition introduces even more disorder, enhancing the VRH effect.

Additional support for 2D VRH is obtained by exploring the reasonableness of length scales derived from the fit. In 2D VRH, the localization length, a, is set by $k_B T^* \approx (N(E_F) a^2 t)^{-1}$ where $N(E_F)$ is the density of localized states at E_F.[16] A plausible assumption $N(E_F) = 10^{20}\ eV^{-1}cm^{-3}$ gives a reasonable 8 Å estimate for a. We can also estimate the optimum hopping range, R, which for 2D VRH should be greater than t (thickness of the 2D region) but smaller than the confined area. From TEM, the interface between the NW and the FIB-Pt contact is $\sim 100 \times 500\ nm^2$, so $3\ nm < R < 100$ nm delimits the sensible length scale. Using $R \approx a(T^*/T)^{1/3}$, we obtain 6−12 nm in the range $40 < T < 300$ K, again consistent with 2D VRH.

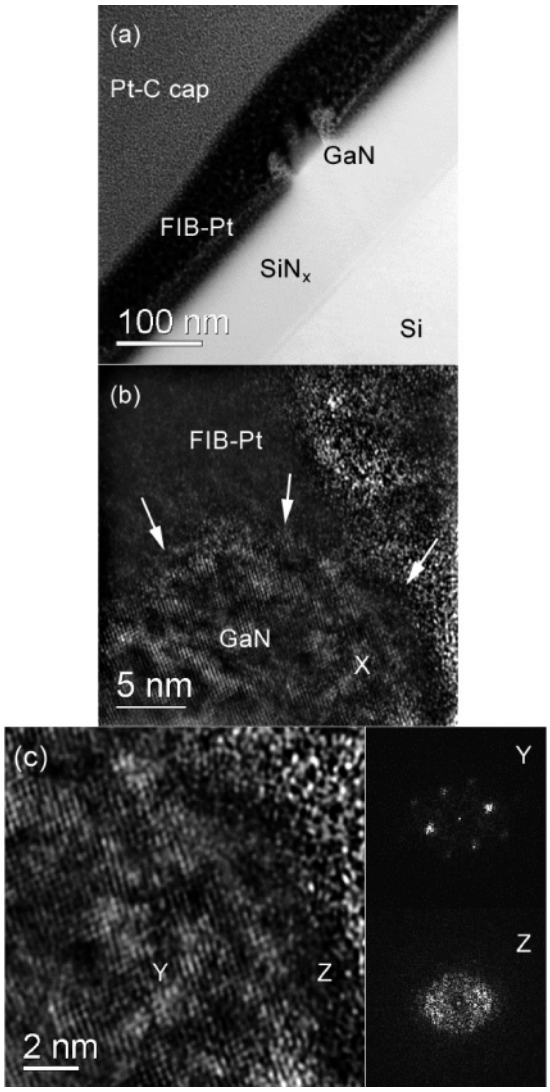

Figure 3. Cross-sectional TEM images from the FIB-Pt contact. The specimen is prepared by low-current Ga ion-beam sectioning. A protective Pt-C capping layer is e-beam deposited in the FIB system prior to sectioning. (a) Typical bright-field (BF) low-resolution STEM image of the contact area. Two bright areas beside the NW are C-rich Pt as confirmed by electron energy loss spectroscopy (not shown); the carbon originates from the organo-Pt precursor. (b) High-resolution BF TEM image revealing the interface between the FIB-Pt contact and the underlying GaN NW. A band of amorphous GaN is noted along the interface, indicated by white arrows. (c) Magnified view of the interface area centered about X in (b). The disturbed GaN lattice (Y) and the amorphized GaN at the interface (Z) are clearly visualized and corroborated from selected area electron diffraction: diffuse spots from the Y and amorphous ring from Z.

In summary, FIB-Pt contacts on large-diameter GaN NW exhibit Schottky barrier behavior but with unusually low barrier heights. This is attributed to E_F pinning by localized states in FIB-amorphized GaN under the contacts and is corroborated by cross-sectional TEM. Contacts to small NWs

are ohmic, but the transport is limited by 2D VRH at all T values studied (40−300 K). The two-probe ρ at 300 K are 0.04, 1.6, 1.3, and 6.4 Ωcm for d = 66, 120, 140, and 184 nm, respectively. The onset of VRH in the smallest NW is attributed to the increased fraction of amorphous GaN under the contact. The detailed and unique nature of the FIB-Pt contact process suggests interesting applications that exploit the local property modulation in nanostructures by beam-induced structure and morphology modification.

Acknowledgment. This work was supported by USDOE grant no. DE-FG02-98ER45701 (C.Y.N.). We also acknowledge the use of shared facilities supported by NSF/MRSEC: DMR02-03378 (D.T.). We are grateful to Jay Kikkawa for the use of his low-temperature transport facility.

References

(1) Xia, Y.; Yang, P.; Sun, Y.; Wu, Y.; Mayers, B.; Gates, B.; Yin, Y.; Kim, F.; Yan, H. *Adv. Mater.* **2003**, *15*, 353.
(2) Nakamura, S.; Fasol, G. *The Blue Laser Diode*; Springer: Berlin, 1997.
(3) Mishra, U. K.; Parikh, P.; Wu, Y.-F. *Proc. IEEE* **2002**, *90*, 1022.
(4) Uenoyama, T. *Phys. Rev. B* **1995**, *51*, 10228.
(5) Han, W.; Fan, S.; Li, Q.; Hu, Y. *Science* **1997**, *277*, 1287.
(6) Johnson, J. C.; Choi, H.-J.; Knutsen, K. P.; Schaller, R. D.; Yang, P.; Saykally, R. J. *Nat. Mater.* **2002**, *1*, 106.
(7) Huang, Y.; Duan, X.; Cui, Y.; Lieber, C. M. *Nano Lett.* **2002**, *2*, 101.
(8) Zhong, Z.; Qian, F.; Wang, D.; Lieber, C. M. *Nano Lett.* **2003**, *3*, 343.
(9) Qian, F.; Li, Y.; Gradecak, S.; Wang, D.; Barrelet, C. J.; Lieber, C. M. *Nano Lett.* **2004**, *4*, 1975.
(10) Nam, C. Y.; Kim, J. Y.; Fischer, J. E. *Appl. Phys. Lett.* **2005**, *86*, 193112.
(11) Nam, C. Y.; Tham, D.; Fischer, J. E. *Appl. Phys. Lett.* **2004**, *85*, 5676.
(12) Wang, L.; Nathan, M. I.; Lim, T.-H.; Khan, M. A.; Chen, Q. *Appl. Phys. Lett.* **1996**, *68*, 1267.
(13) Götz, W.; Johnson, N. M.; Chen, C.; Liu, H.; Kuo, C.; Imler, W. *Appl. Phys. Lett.* **1996**, *68*, 3144.
(14) Van de Walle, C. G.; Neugebauer, J. *J. Appl. Phys.* **2004**, *95*, 3851.
(15) Sze, S. M. *Physics of Semiconductor Devices*; Wiley: New York, 1981.
(16) Mott, N. F. *Conduction in Non-Crystalline Materials*; Clarendon Press: Oxford, 1993.
(17) Vavro, J.; Kikkawa, J. M.; Fischer, J. E. *Phys. Rev. B* **2005**, *71*, 155410.
(18) Look, D. C. *Mater. Sci. Eng., B* **1997**, *50*, 50.
(19) Dhara, S.; Datta, A.; Wu, C. T.; Lan, Z. H.; Chen, K. H.; Wang, Y. L.; Chen, Y. F.; Hsu, C. W.; Chen, L. C.; Lin, H. M.; Chen, C. C. *Appl. Phys. Lett.* **2004**, *84*, 3486.
(20) Dhara, S.; Datta, A.; Wu, C. T.; Lan, Z. H.; Chen, K. H.; Wang, Y. L.; Chen, L. C.; Hsu, C. W.; Lin, H. M.; Chen, C. C. *Appl. Phys. Lett.* **2003**, *82*, 451.
(21) Look, D. C. *Appl. Phys. Lett.* **2003**, *83*, 3525.
(22) Hashizume, T.; Nakasaki, R. *Appl. Phys. Lett.* **2002**, *80*, 4546.
(23) Stumm, P.; Drabold, D. A. *Phys. Rev. Lett.* **1997**, *79*, 677.
(24) Koo, A.; Lanke, U. D.; Ruck, B. J.; Brown, S. A.; Reeves, R.; Liem, I.; Bittar, A.; Trodahl, H. J. *Mater. Res. Soc. Symp. Proc.* **2002**, *693*, I10.10.
(25) Tham, D.; Nam, C. Y.; Fischer, J. E., submitted for publication.

NL0515697